Small-Angle X-ray Scattering Study of Lamellar Microdomains in Diblock Copolymers in the Weak Segregation Regime

T. Wolff, C. Burger, and W. Ruland*

Fachbereich Physikalische Chemie und Zentrum für Materialwissenschaften, Philipps-Universität Marburg, Postfach, D-35032 Marburg, Germany

Received September 29, 1993; Revised Manuscript Received February 9, 1994®

ABSTRACT: The lamellar structure of a nearly symmetric diblock copolymer in the weak segregation regime is investigated using small-angle X-ray scattering (SAXS). The scattering curves measured at room temperature are analyzed using the concept of the interface distribution functions. The determination of the interfacial thickness shows that an additional component of the scattering function has to be taken into account to obtain values comparable to theoretical ones. This component which has so far been neglected in similar studies is due to the statistical structure of the domain boundary. The temperature dependence of the interfacial thickness and of the lattice constant, obtained using synchrotron SAXS from room temperature up to the microphase separation transition (MST), is in fair agreement with recently published theories.

1. Introduction

In a recent paper,[1] we reported temperature-dependent small-angle X-ray scattering (SAXS) measurements in the vicinity of the microphase separation transition (MST) for a nearly symmetric diblock copolymer. We have shown that the intensity distributions in the disordered phase can be completely reproduced using the appropriate theories. This is possible since the intensity distributions in the disordered phase are quantitatively determined by essentially two free parameters, the parameter $\alpha = 2(\chi N)_s - \epsilon$ and the radius of gyration R_g. For the ordered phase, the situation is different. In the vicinity of the MST, theories based on the assumption of strong segregation[2,3] and the narrow interface approximation (NIA)[4-7] are not applicable. Leibler[8] predicted that the density distribution in the ordered phase near the MST is represented by waves with wavelengths corresponding to the periodicity of the long-range order. A lamellar macrolattice near the MST should thus be described by a single wave with the wavelength L. With increasing distance from the MST the segregation is expected to develop a morphology with more neatly defined domains and domain boundaries.

Recently, Bates, Rosedale, and Fredrickson[9] have discussed the difference in the morphology of lamellar structures near the MST resulting from the mean-field approach with and without fluctuation correction. They claim that the fluctuation produces higher amplitudes of the local variation of the density in the disordered phase and that these density variations are superposed on the long-range order in the ordered phase. However, the effect of fluctuation in the disordered phase *reduces* the amplitude of the local variations of the density in the disordered state since the fluctuation correction leads to *lower* values of the structure factor $S(q)$ as compared to the mean-field result. There is thus no basis for the assumption of a superposition of a "spinodal-like" density fluctuation on the long-range order in the ordered phase.

The aim of this paper is to show that a reliable quantitative interpretation of the SAXS of lamellar systems near the MST (weak segregation regime) is possible if precise measurements are carried out over the entire range of the scattering angles accessible to SAXS. The structural parameters to describe such systems are the statistics of the lamellar structure and the width and the statistical structure of the domain boundaries. The statistics of the lamellar structure can be determined using the concept of interface distribution functions.[10] The correct determination of the width of the interfacial boundary depends not only on the quantitative separation of the SAXS from the background due to thermal density fluctuations[1] but also on the determination of the effect of the statistical structure of the domain boundary[12] which has so far been neglected in other experimental studies.[13-15] The combined application of these methods of evaluation results in a phenomenological description of the structure in the weak segregation regime which should facilitate the development of a more involved theoretical treatment of this state.

2. Lamellar Two-Phase Systems

2.1. Structural Parameters. We first consider an idealized lamellar two-phase system with sharp boundaries and planar interfaces as shown in Figure 1a.

The scattering of such a structure is determined by the statistics of the thicknesses of the lamellae as well as the finite size of the stacks. If the evaluation of the scattering is limited to the angular range of the first-order maximum, the separation of these effects is not possible. The wider the angular range and the more precise the measurements at higher angles, the more detailed and reliable are the results of the evaluation.

There are two simple models which can describe the statistics of a stack of lamellae. The first one is the "stacking model" in which the statistics of the lamellar stack is determined by the distributions $h_1(d_1)$ and $h_2(d_2)$ of the thicknesses of the two lamellae d_1 and d_2. These distributions are considered to be statistically independent; i.e., there is no correlation between the two variances σ_1^2 and σ_2^2. The period L is given by $L = d_1 + d_2$.

The other model is the "lattice model" which was first proposed by Tsvankin.[17] Here the statistics of the stack is determined by the variance σ_1^2 of one of the lamellae and σ_L^2 of the period L which is in this case considered to be the distance between the centers of two lamellae of one kind.

If the interfaces of the lamellae are completely planar as shown in Figure 1a and the lateral dimensions are large compared to the thicknesses of the lamellae, the total interface area per volume S_0/V is given by

$$S_0/V = 2/L$$

* To whom correspondence should be addressed.
® Abstract published in *Advance ACS Abstracts,* April 15, 1994.

0024-9297/94/2227-3301$04.50/0

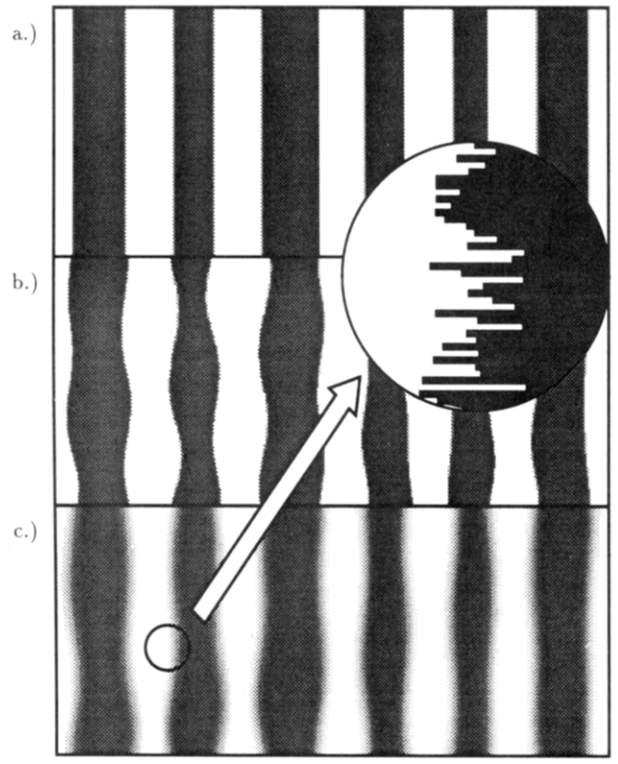

Figure 1. Schematic representation of a lamellar two-phase system with sharp boundaries (a), with sharp boundaries and nonplanar interfaces (b), and with nonplanar interfaces and an interfacial boundary of finite width (c). The inset shows an enlarged part of the interfacial boundary (small circle) in which the statistical structure is represented by "fingers".

If the interfaces are not planar as shown in Figure 1b, the total interface area S obtained from l_p is larger than S_0 obtained from L. l_p is the average chord length parameter and is related to the total interface S by

$$l_p = \frac{4c(1-c)V}{S}$$

c is the volume fraction of one phase. The ratio

$$\frac{S}{S_0} = \frac{2c(1-c)L}{l_p} = \frac{2d_1d_2}{Ll_p} \tag{1}$$

is a measure of the planarity of the interfaces.[19]

Figure 1c shows the lamellar two-phase system with nonplanar interfaces and an interfacial boundary with a finite width. An enlarged part of the domain boundary is shown in the inset to demonstrate the statistical structure of it. The model used to describe the local morphology of the interface is explained in section 5.

2.2. SAXS of a Lamellar Structure. For a randomly oriented two-phase system with sharp boundaries, Porod's law in 3D is given by[16]

$$\lim_{s\to\infty} s^4 I(s) = k/2\pi^3 l_p \tag{2}$$

where $s = q/2\pi = 2\sin(\theta/\lambda)$, θ is the Bragg angle, λ is the wavelength, I is the scattered intensity, and k is the invariant

$$k = V(\rho_1 - \rho_2)^2 c(1-c) = 4\pi \int_0^\infty s^2 I(s)\, ds$$

ρ_n is the average electron density of phase n.

Only assuming the distributions $h_1(d_1)$ and $h_2(d_2)$ to be normalized, one finds for the scattering intensity for the stacking model[18] (infinite stack size)

$$I(s) = \frac{k}{4\pi^3 s^4} \mathrm{Re}\left[\frac{(1-H_1(s))(1-H_2(s))}{1-H_1(s)\,H_2(s)}\right] \tag{3}$$

where H_n is the 1D Fourier transform of h_n and Re stands for the "real part". The lattice model gives

$$I(s) = \frac{k}{4\pi^3 s^4}\left\{1 - \mathrm{Re}[H_1(s)] + 4[\mathrm{Im}[H_1(s/2)]]^2\, \mathrm{Re}\left[\frac{H_L(s)}{1-H_L(s)}\right]\right\} \tag{4}$$

where H_L is the Fourier transform of the distribution h_L of L and Im stands for the "imaginary part". h_L can also be any normalized distribution.

3. Interface Distribution Functions

In an earlier work,[10] the interface distribution function $g_1(r)$ for lamellar systems has been introduced. It is defined by the second derivative of the autocorrelation function for positive definite values of the distance r in real space and can be computed by inverse Fourier transformation $\mathcal{F}_1^{-1}$ of the interference function $G_1(s)$

$$g_1(r) = \mathcal{F}_1^{-1}[G_1(s)], \quad G_1(s) \propto [\lim_{s\to\infty} s^4 I(s)] - s^4 I(s) \tag{5}$$

To obtain $g_1(r)$ from slit-smeared scattering curves, an equivalent to G_1 has been defined,[10]

$$\tilde{G}_1(s) \propto [\lim_{s\to\infty} s^3 J(s)] - s^3 J(s) \tag{6}$$

where $J(s)$ is the intensity smeared with a slit of infinite length. An expression for $g_1(r)$ has been derived which is a combination of inverse Fourier transformation and slit desmearing. It can be simplified to the following form:

$$g_1(r) \propto \int_0^\infty \tilde{G}_1(s)\left(4J_0(2\pi rs) - \frac{(1+4\pi^2r^2s^2)}{\pi rs} J_1(2\pi rs)\right) ds \tag{7}$$

where J_n is the Bessel function of the first kind of the nth order. The interface distribution function can be written in the form[10]

$$g_1(r) \propto h_1 + h_2 - h_{12} - h_{21} + h_{121} + h_{212} - h_{1212} - h_{2121} + \ldots - \ldots$$

In the limit of infinite stack size, h_i are normalized distributions of the distances between interfaces measured perpendicular to the planes of the lamellae. Finite stack size leads to decreasing weights of the distributions h_n with increasing distance. This can be taken into account by a function of the type $g_1(r)\exp(-r/l)$ where l is the average stack size.

4. Width of the Interfacial Boundary

Interfacial boundaries of finite width produce an attenuation of the scattering intensity[20] which can be represented by

$$I = I_{id} H_z^2$$

where I_{id} is the scattering intensity of an ideal two-phase system (sharp boundaries) and H_z is the Fourier transform of the "smoothing" function h_z. For slit-smeared intensity distributions J in the range of validity of Porod's law, one finds[20]

$$J = J_{id}F$$

where

$$F = \frac{2}{\pi}s^3\int_{-\infty}^{\infty}\frac{H_z^2[(s^2+y^2)^{1/2}]}{(s^2+y^2)^2}\,dy \quad (8)$$

If h_z is a normalized Gaussian distribution, $H_z = \exp(-\pi d_z^2 s^2)$ where d_z is the width of the interfacial boundary and

$$f_{erf}(d_z s) = (1 - 4\pi d_z^2 s^2)\,\mathrm{erfc}[(2\pi)^{1/2}d_z s] + 8^{1/2}d_z s\exp(-2\pi d_z^2 s^2) \quad (9)$$

where erfc = 1 − erf and $\mathrm{erf}(x) = 2\pi^{-1/2}\int_0^x \exp(-t^2)\,dt$.

Using the NIA, Helfand and Wasserman[4] find the relationship

$$d_z = 2b/(6\chi)^{1/2} \quad (10)$$

for interfaces in phase-separated block copolymers and polymer mixtures. χ is the Flory–Huggins interaction parameter and b the segment length. Furthermore, the attenuation function is given by

$$H_z = (\pi^2 d_z s/2)\,\mathrm{csch}(\pi^2 d_z s/2) \quad (11)$$

The corresponding $F_{th}(d_z s)$ is obtained using eqs A-7 and A-8 given in Appendix A. A comparison of $F_{erf}(d_z s)$ with $F_{th}(d_z s)$ shows a difference of about 5% in the determination of d_z in the range of $d_z s$ values of practical interest. Nevertheless, in this work we use $F_{th}(d_z s)$ for the evaluation since this avoids unnecessary errors in a direct comparison between our experimental results and the theory of Helfand and Wasserman.

Mean-field calculations carried out by Shull[21] indicate that the result of Helfand and Wasserman is only reached at the limit $\chi N \to \infty$. In a recent paper, Semenov[3] has extended the theory of Helfand and Wasserman by calculating corrections due to higher-order terms in a gradient expansion of the free energy. This study leads to the relationship

$$d_z = \frac{2b}{(6\chi)^{1/2}}[1 + 1.34(\chi N)^{-1/3}] \quad (12)$$

5. Statistical Structure of the Domain Boundary

The local fluctuation of the concentrations of phase 1 and phase 2 within the domain boundary produces a supplementary component of the scattering intensity. To assess the effect of the statistical structure of the domain boundary, a simplified model[12] was introduced in which the local morphology of the interface is represented by "fingers" with cross section $A_0 = \pi R_0^2$. Using this model and the Gaussian approximation for H_z, the following expression has been derived for the scattering of a statistical boundary structure[12]

$$I_z(s) = \frac{(\rho_1 - \rho_2)^2 S A_0 d_z^2}{2\pi} G_\omega^{erf}(s) \quad (13)$$

where

$$G_\omega^{erf}(s) = \frac{1}{b}\left\{\exp(-b) - 1 + 2\exp(-a)\left[\frac{(a\pi)^{1/2}}{2}\,\mathrm{erfi}(\sqrt{a}) + \frac{[(b-a)\pi]^{1/2}}{2}\,\mathrm{erf}[(b-a)^{1/2}]\right]\right\}$$

with $a = (\pi R_0 s)^2$ and $b = 2\pi(d_z s)^2$. $\mathrm{erfi}(x) = -i\,\mathrm{erf}(ix)$ and S is the total interface. The corresponding I_z using the H_z of Helfand and Wasserman is given by eq B-1 in Appendix B. Numerical calculations using the experimental length profile of the primary beam are performed to obtain J_z, the equivalent of I_z in slit-smeared SAXS.

6. Thermal Density Fluctuations

The finite compressibility of the sample produces a supplementary SAXS intensity component I_{Fl} which, for many polymers, can be approximated by[22]

$$I_{Fl}(s) = a + bs^2$$

Slit smearing with a finite slit length only changes the values of the constants a and b. In some cases, b is small and can be neglected.[11] In other cases, a better fitting is obtained using the approximation[22]

$$J_{Fl}(s) = ae^{bs^2}$$

7. Experimental Section

The sample investigated is a poly(styrene-*b*-butadiene) diblock copolymer, synthesized via anionic living polymerization. The molecular weight characteristics as obtained by GPC are as follows: total molecular weight $M_{w,sb}$, 18 000; molecular weight of the styrene block $M_{w,s}$, 9000; total polydispersity U_{sb}, 0.09; polydispersity of the styrene block U_s, 0.070, where the polydispersity U is defined as $U = M_w/M_n - 1$. The polydispersity of the butadiene block is obtained assuming independent statistics of the two block lengths. From these data one derives a degree of polymerization $N = 229$, and a composition $f_s = 0.47$, based on the volume fraction of the styrene block.

The SAXS measurements at room temperature were made with a Kratky camera. The time-resolved synchrotron SAXS measurements were performed at DESY in Hamburg, Germany.

8. Results and Discussion

8.1. Determination of the Interfacial Thickness.

To determine the interfacial thickness d_z from a slit-smeared intensity distribution J measured with a Kratky camera at room temperature, we first neglect the contribution of J_z and consider the relationship

$$\tilde{G}_1(s) = 1 - \frac{4\pi^2 s^3 l_p(J(s) - J_{Fl}(s))}{kF_{th}(d_z s)} \quad (14)$$

We use a trial-and-error method developed earlier[11] in which the values of J_{Fl} and d_z are varied with the condition that the interference function $\tilde{G}_1$ is oscillating about zero (Porod's law) and that the integral over $\tilde{G}_1$ is nearly zero. The latter condition results from the requirement $g_1(0) = 0$ valid for lamellar systems. This method is used together with the approximations for the fluctuation background referred to in the theoretical section. Figure 2 shows the interference function for a fluctuation background of the form $J_{Fl} = 16.3 + 820s^2$. The results are shown in Table 1. To compare the values of d_z obtained in this way with theoretical values, we compute the interfacial thickness d_z using eqs 10 and 12. The results are $d_z = 21.5$ Å and $d_z = 33.4$ Å, respectively. The value of χ is calculated from the results of a synchrotron SAXS study of the disordered phase of the same sample[1] ($\chi = -9.6 \times 10^{-4} + 18.78/T$) and $b = 6.59$ Å ($\rho_0 b^2 = \rho_S b_S^2/2 + \rho_B b_B^2/2$, $\rho_0 = (\rho_S\rho_B)^{1/2}$, $b_S = 6.8$ Å, $b_B = 6.3$ Å). Inspection of Table 1 shows that the choice of the type of the fluctuation background has little influence on the values of l_p, S/S_0, and d_z. The values of S/S_0 have been calculated using eq 1 and the structural parameters given in the next subsection. They show that the interface of the lamellae is not planar.

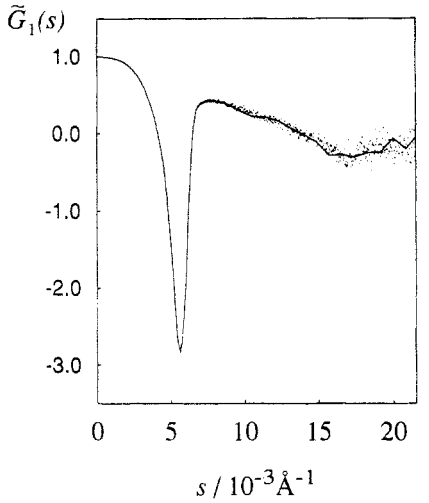

Figure 2. Interference function $\tilde{G}_1(s)$ (dots) *without* J_z correction for a fluctuation background $J_{Fl} = 16.3 + 820s^2$. The solid curve is a smoothing cubic spline. The increase of the statistical deviations at large values of s are due to the multiplication by s^3.

Table 1. Structural Parameters Obtained Neglecting the Statistical Structure of the Domain Boundaries

$J_{Fl}(s)$/cps	d_z/Å	l_p/Å	S/S_0
16.5	6.5	66.4	1.20
$16.3 + 820\ s^2$	6.2	64.5	1.24
$16.3 \exp(42.5s^2)$	6.2	64.6	1.24

Table 2. Structural Parameters Obtained Taking into Account the Statistical Structure of the Domain Boundaries

$J_{Fl}(s)$/cps	d_z/Å	R_0/Å	l_p/Å	S/S_0
14.5	24	33	65.9	1.18
$14 + 800\ s^2$	25.5	35	67.2	1.15
$14 \exp(41.5s^2)$	25.5	35	67.4	1.15

The essential result is that the d_z values obtained experimentally using eq 14 are far lower than the theoretical ones predicted from eq 10 or 12. Larger values of d_z can only be obtained if an additional component of the scattering curve is taken into account which, in contrast to J_{Fl}, increases in intensity toward small angles. We consider this component to be due to the scattering from the statistical structure of the domain boundary.[12] This leads to the relationship

$$\tilde{G}_1(s) = 1 - \frac{4\pi^2 s^3 l_p (J(s) - J_{Fl}(s) - J_z(s))}{kF_{th}(d_z s)} \qquad (15)$$

We obtain $J_z(s)$ from $I_z(s)$ according to eq B-1 and subsequent smearing with the experimental slit-length profile. Using the same conditions for the trial-and-error method as given above, we obtain the results listed in Table 2. The resulting interference function is plotted in Figure 3. Again, the choice of the function representing the fluctuation background has little influence on the parameters. However, the d_z values are about 4 times larger than those shown in Table 1 and much closer to the theoretical ones predicted using eq 10. On the other hand, the values of l_p and S/S_0 are not changed significantly. Since J_z depends on d_z and R_0, we obtain the latter as a supplementary parameter from the fitting. It is of interest to note that R_0 is found to be larger than d_z.

8.2. Characterization of the Lamellar Structure. After the determination of $\tilde{G}_1(s)$, the interface distribution function $g_1(r)$ is computed according to eq 7. To eliminate the influence of the width of the primary beam on the higher order peaks of $g_1(r)$, the experimental scattering curve is slit-width desmeared using the method proposed by Svergun, Semenyuk, and Feigin.[23] Figures 4 and 5 show curves of $g_1(r)$ computed without and with the J_z correction, respectively, together with theoretical curves. The com-

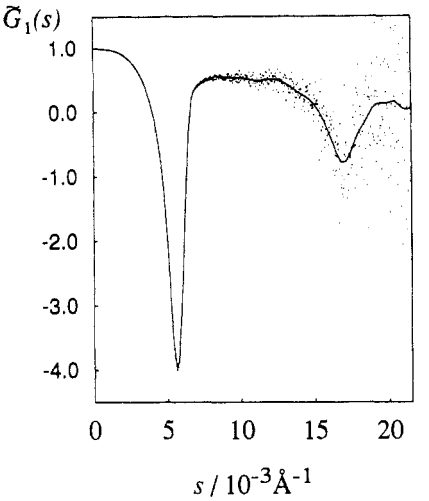

Figure 3. Interference function $\tilde{G}_1(s)$ (dots) *with* J_z correction for a fluctuation background $J_{Fl} = 14 + 800s^2$. The solid curve is a smoothing cubic spline. The increase of the statistical deviations at large values of s is due to the multiplication by s^3.

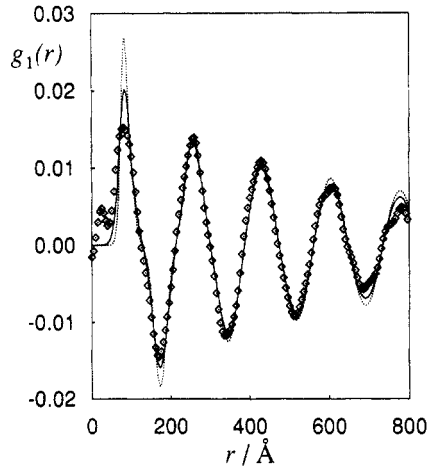

Figure 4. Interface distribution function computed from the experimental values (◇) *without* J_z correction. The dotted line is the theoretical curve according to the stacking model and the solid line that according to the lattice model.

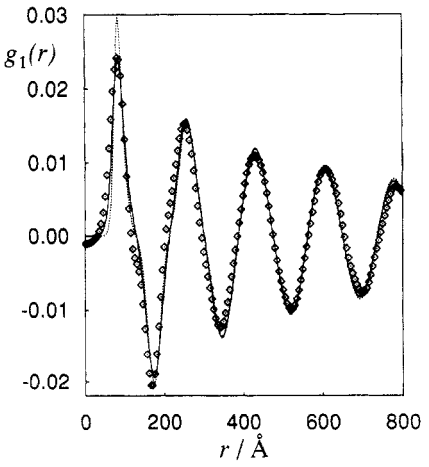

Figure 5. Interface distribution function computed from the experimental values (◇) *with* J_z correction. The dotted line is the theoretical curve according to the stacking model and the solid line that according to the lattice model.

Table 3. Structural Parameters of the Lamellar System

	L/Å	σ_L/Å	d_1/Å	σ_1/Å	d_2/Å	σ_2/Å
a	173.5	18.4	81.6	8.2	91.9	13.8
b	173.5	17.4	81.6	12.2	91.9	19.4
c	174	17.4	81.8	12.3	91.2	19.4

[a] From $g_1(r)$, stacking model. [b] From $g_1(r)$, lattice model. [c] From $J(s)$, lattice model.

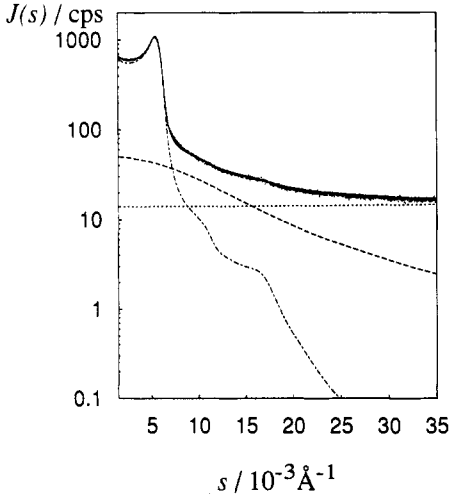

Figure 6. Plot of the experimental scattering curve (dots) and the fit to the theoretical scattering function (solid line). The dash-dotted curve is the scattering from the lamellar system, the dashed curve is the scattering from the statistical structure of the domain boundary, and the dotted curve is the fluctuation background.

parison of the two figures shows that the influence of the effect of the statistical structure of the domain boundary on $g_1(r)$ is negligible.

Using the stacking model for the interpretation of the curves leads to variances of the lamellar thicknesses which are similar to the values of the polydispersities of the homopolymer blocks. However, especially in Figure 5, the height of the first peak is too large in comparison with the experimental value. The theoretical curves corresponding to the lattice model show a somewhat better agreement. No improvement of the evaluation of $g_1(r)$ could be obtained by considering a finite stack size. All values obtained from the evaluation of $g_1(r)$ are given in Table 3 (row *a*, stacking model; row *b*, lattice model).

Since d_z and the intensity components $J_{Fl}(s)$ and $J_z(s)$ have already been determined, we can compare the experimental scattering curve with the sum of the three components $J_{Fl}(s)$, $J_z(s)$, and $J_{lam}(s)$ $F_{th}(d_z s)$, where $J_{lam}(s)$ is the slit-smeared equivalent to the intensity distribution defined by eq 4. The best fit is obtained using the parameters given in Table 3, row c. This comparison is of interest since intensity distributions are, in general, affected differently by variations of structural parameters than the corresponding Fourier transforms. The comparison shows that the evaluations of $g_1(r)$ and $J(s)$ are consistent. In Figure 6, the experimental scattering curve is plotted together with the sum and the individual curves of the three components. A logarithmic scale is used for the intensity in order to demonstrate the requirements of accuracy for such studies. It is of interest to note that the components $J_{Fl}(s)$ and $J_z(s)$ are dominant in a large range of s values and that they can be neglected only in the vicinity of the first-order maximum of the interference function.

8.3. Temperature Dependence of Structural Parameters. Since a quantitative evaluation of scattering curves as presented above would be impractical for a large amount of data, we have limited the evaluation of the 40 scattering curves we measured with synchrotron radiation in the range from room temperature up to the MST to the determination of the temperature dependence of the period L, the variance σ_L, and the interfacial with d_z, using the corresponding parameters obtained at room temperature as standard and the lattice model to relate the width of the first-order maximum to σ_L. Since the prefactor s^{-4} in eq 4 shifts the position of the maximum s_{max} to values smaller than $s_{max} \simeq 1/L$, we take the values for the period L from the peak position in a plot of $s^4 I_{exp}$ vs s where I_{exp} is the measured synchrotron SAXS intensity. A plot of $s^4 I_{exp}$ vs s for the initial temperature and a profile fitting is shown in the inset of Figure 7. The result of this evaluation is shown in Figure 8 where L is plotted vs χ (lower axis) and T (upper axis) together with theoretical data (NIA) calculated according to Helfand and Wasserman[4] and to Semenov.[2] There is a slight difference between the values for the heating and the cooling cycle, but the general trend is a slowly increasing value, probably due to thermal expansion, up to about 70 °C followed by a decrease with increasing temperature as expected from

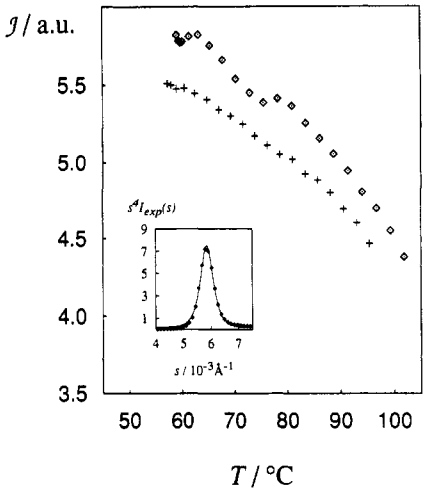

Figure 7. Integral intensity $J = \int s^4 I_{exp}\, ds$ vs T for heating (◇) and the cooling cycle (+). To obtain more accurate values for J, the peak is fitted by a sech(s) (inset: plot of $s^4 I_{exp}$ vs $10^3 s$ (dots) and the fit (solid line) for T = 59.1 °C, synchrotron SAXS).

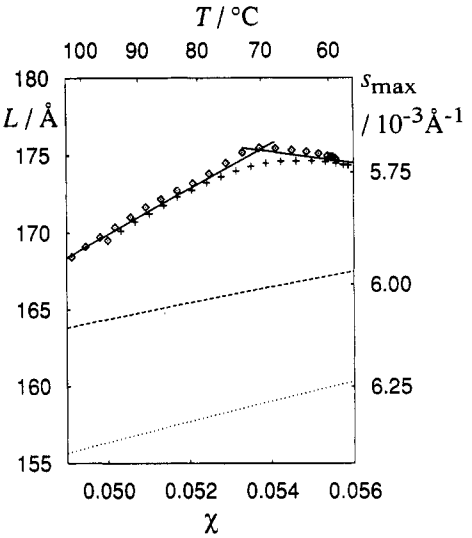

Figure 8. Period L (left axis) and the corresponding s_{max} (right axis) vs χ (lower axis) and T (upper axis) for the heating (◇) and the cooling cycle (+). The point of intersection of the solid lines at χ = 0.0537 belongs to a temperature of 70.3 °C which we interpret as the glass temperature of the polystyrene domains. The dashed line is the theoretical L according to Semenov[2] and the dotted line that according to Helfand and Wasserman.[4]

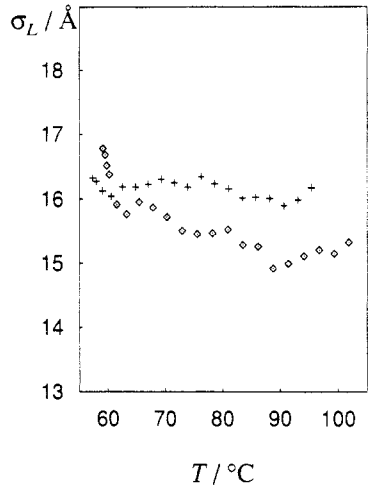

Figure 9. Variance σ_L of the period L vs T for the heating (◇) and the cooling cycle (+).

the theory. The change of slope at about 70 °C is most probably due to the glass transition of the polystyrene domains which stabilizes a nonequilibrium structure. If we accept this interpretation, the glass temperature of the polystyrene domains is about 70 °C which is 20 °C below T_g of a homopolymer polystyrene with the same molecular weight as the polystyrene blocks. The decrease of T_g can be explained by a plastification of the domains due to the weak segregation. From the region above T_g we obtain the scaling law $L \propto \chi^{\alpha}$ with $\alpha = 0.44$. This value of α obtained for the weak segregation regime is much larger than the corresponding theoretical values for the strong segregation regime. With the χ values used in this work, $\alpha = 0.221$ is calculated from the program of Helfand and Wasserman.[4] The analytical theory of Semenov[2] predicts $\alpha = 1/6$. It is of interest to note that the value of α determined in this work is similar to that predicted by Shull[21] using a mean-field approach.

To determine σ_L and $d_z(T)$, we measure the temperature dependence of the integral intensity $\mathcal{J} = \int s^4 I_{exp}\, ds$ and of the integral width $B_{int} = \mathcal{J}/(s_{max}^4 I_{exp}(s_{max}))$ of the first-order maximum of the $s^4 I_{exp}$ curve. If we assume the ratio σ_L/σ_1 to be temperature independent, we find the approximation $\sigma_L = (1.9 \times 10^4\ \text{Å}^2) B_{int} + 7.7$ Å from calculations of the integral width as a function of σ_L, using the lattice model and the experimental values of σ_L and σ_1 at room temperature as standard. Figure 9 shows the values of σ_L as a function of temperature. The plot shows that σ_L stays nearly constant over the whole observed temperature range; i.e., the statistics of the lamellar system do not change significantly in this range. Since the scattering intensity is corrected for absorption and variations of the primary beam intensity, the integral intensity of the first-order maximum of $s^4 I_{exp}$ is given by

$$\mathcal{J} \propto (\rho_S - \rho_B)^2 H_z^2(s_{max}) \mathcal{J}_{id} \qquad (16)$$

ρ_S and ρ_B are the electron densities of polystyrene and polybutadiene, respectively, H_z is the attenuation function defined by Helfand and Wasserman (eq 11), and $\mathcal{J}_{id}$ is the integral intensity of the first-order maximum of the $s^4 I_{id}$ curve, where I_{id} is the scattering function of a lamellar system with sharp boundaries. To obtain $d_z(T)$, we solve the following equation with an iterative method for each temperature

$$\frac{\mathcal{J}}{(\rho_S - \rho_B)^2 \mathcal{J}_{id}} - A\frac{\pi^4 d_z^2 s_{max}^2}{4} \operatorname{csch}^2(\pi^2 d_z s_{max}/2) = 0 \qquad (17)$$

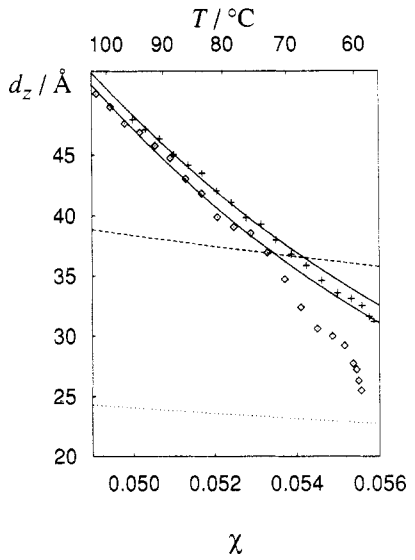

Figure 10. Interfacial thickness d_z vs χ (lower axis) and T (upper axis) for the heating (◇) and the cooling cycle (+). The solid lines are fits to $d_z(\chi) \propto \chi^{-\beta}$. The dashed line is the theoretical d_z according to eq 12 and the dotted line that according to eq 10.

$\mathcal{J}_{id}$ is calculated using the values for σ_L and σ_1 obtained from B_{int} and the experimental values for L. We use the values of the mass density and the thermal expansion coefficients given in the literature[24] for the calculation of $(\rho_S - \rho_B)^2$, taking into account the change at T_g. Since d_z has already been determined at room temperature, we use this value as reference to obtain A. In Figure 10, d_z is plotted as a function of T and of χ. We obtain a slight change of slope at about 70 °C which can, as in the case of the temperature dependence of L, be explained by the glass transition of the polystyrene domains. Considering a scaling law of the type $d_z \propto \chi^{-\beta}$ at temperatures above 70 °C, we find $\beta = 3.7$ for the heating cycle and $\beta = 3.5$ for the cooling cycle which is an order of magnitude larger than $\beta = 0.5$ valid for the NIA. It is of interest to note that d_z appears to be markedly smaller if one of the phases is below T_g.

9. Conclusions

The present study shows that it is possible to obtain a quantitative interpretation of the SAXS of diblock copolymers in the weak segregation regime using general evaluation methods for two-phase systems, in particular for lamellar systems, already reported in the literature.

Values of the interfacial thickness d_z close to theoretically predicted ones are obtained only if the scattering from the statistical structure of the domain boundary J_z is taken into account. The effect of J_z is also important for a better agreement between experimental and theoretical scattering curves.

The temperature dependence of d_z is much stronger than that predicted for the strong segregation regime. This result is predicted by theoretical calculations of McMullen[25] and Melenkevitz and Muthukumar.[26] The temperature or χ dependence of the period L determined in this work can be compared with theoretical predictions of Shull[21] and Mayes and Olvera de la Cruz.[27] In particular, the scaling law for L near the critical point predicted by Shull[21] is very similar to that found in this work.

It appears, however, to be necessary to improve the approach for the statistical structure of the domain boundary since the evaluation leads to values of R_0 which exceed the range of validity of the approximations used in the model. Recently, Semenov[28] has derived a theory

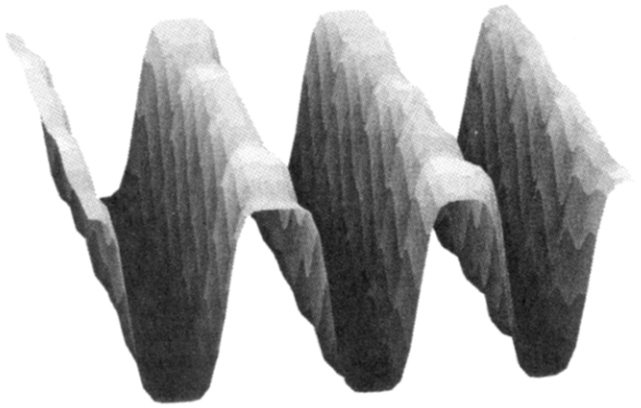

Figure 11. Schematic representation of the density distribution in the lamellar system at room temperature. The deviations from the ideal structure correspond to the experimentally determined values of d_z and S/S_0.

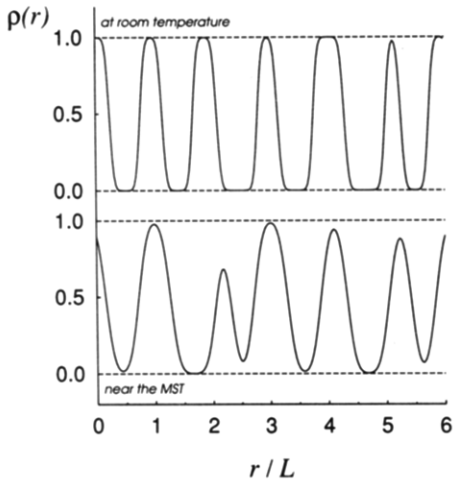

Figure 12. Density profile showing the statistical fluctuations of the thicknesses of the lamellae and the periodicity as obtained from the experimental data. The upper curve refers to room temperature and the lower curve to a temperature just below MST.

dealing with the statistical structure of polymer/polymer interfaces, which will be taken into account in future work.

Although the effect of the statistical structure of the domain boundary has a strong influence on the determination of d_z, its influence was found to be negligible on the determination of the statistical parameters describing the lamellar structure.

The lamellar phase shows imperfections which are characterized by variances of the thicknesses of the lamellae and by nonplanar interfaces. A schematic representation of such a structure is shown in Figure 11.

The statistics of the variances as revealed by the interface distribution function are in agreement with a lattice model. This can be explained by assuming the lamellar system to be built up by a spinodal decomposition which predetermines the periodicity of the centers of the lamellae. The effect of finite stack size was found to be negligible.

Figure 12 shows a schematic representation of a section through a lamellar system perpendicular to the interface at room temperature and at a temperature just below MST. The statistics of the lamellar thicknesses and the width of the interface boundaries correspond to those determined in this study. These plots demonstrate clearly the structural features of the microphase separation in the weak segregation regime.

Acknowledgment. We thank Dr. A. N. Semenov for stimulating discussions. The support of part of this work by the Deutsche Forschungsgemeinschaft is gratefully acknowledged.

Appendix A

Let $F(s)$ be defined by eq 8. The prefactor $2\pi^{-1}s^{-3}$ results from the condition $F(0) = 1$. It will be convenient to rewrite eq 8 in the following form.

$$F(s) = \frac{2}{\pi}s^2\int_{s^2}^{\infty}\frac{dt}{(t-s^2)^{1/2}}\frac{H^2(t^{1/2})}{t^2} \qquad \text{(A-1)}$$

If H is Gaussian, the integral (A-1) defines a confluent hypergeometric function of the second kind (see Abramovitz/Stegun 13.2.6[29]) and can be identified in terms of the solution stated in eq 9.

In the general case (A-1) defines a fractional integral of the Weyl type[30] of order $^1/_2$. The solution may possibly be found in the tables. See, e.g., 13.2.(13) in ref 30 for Gaussian H.

For practical calculation it will be convenient to make use of the connection between fractional integrals and Mellin transforms.[30]

$$F(s) = \frac{2}{\pi^{1/2}}\int\frac{dz}{2\pi i}s^{3-2z}\frac{\Gamma(z)}{\Gamma((1/2)+z)}\int_0^{\infty}dt\, t^{z-5/2}H^2(t^{1/2}) \qquad \text{(A-2)}$$

where the contour integral has to be taken along a suitably chosen path.

In order to find the Mellin transform of the squared hyperbolic cosecant, expand into exponentials.

$$x^2\,\mathrm{csch}^2(x) = \frac{4x^2e^{-2x}}{(1-e^{-2x})^2} = 4x^2\sum_{n=1}^{\infty}ne^{-2nx} = \int\frac{dz}{2\pi i}(2x)^{-z}\Gamma(2+z)\,\zeta(1+z) \qquad \text{(A-3)}$$

$\zeta(z)$ is Riemann's ζ-function.

From (A-2) and (A-3) we obtain $F(s)$ in form of the contour integral

$$F(s) = \frac{8}{\pi}\int_{1/2-i\infty}^{1/2+i\infty}\frac{dz}{2\pi i}\left(\frac{\pi^2d_zs}{2}\right)^{-2z}\frac{\Gamma^2((3/2)+z)\,\zeta(1+2z)}{1+z} \qquad \text{(A-4)}$$

To express the solution of this integral in terms of known special functions is probably not easy. However, the integral serves us as a convenient tool to obtain all interesting properties and a computable representation of $F(s)$.

Investigating the integrand of (A-4), we note simple poles at $z = 0$ (due to the ζ-function), at $z = -1$, and also the poles of the squared Γ-function at $z = -^3/_2 - n$; $n = 0, 1, 2, \ldots$ are simple since they coincide with the zeros of the ζ-function. Hence, straightforward residue calculus leads to

$$F(x=\pi^2d_zs/2) = 1 - \frac{2}{3}x^2 + \frac{8}{\pi}x^3\sum_{n=0}^{\infty}x^{2n}\left[\frac{(-1)^n}{n!}\right]^2\frac{2\zeta(-2-2n)}{-1/2-n} \qquad \text{(A-5)}$$

The derivative of the ζ-function in (A-5) can be removed using the following theorem

$$\zeta'(-2-2n) = (-1)^{1+n}\frac{(2+2n)!\zeta(3+2n)}{2^{3+2n}\pi^{2+2n}} \qquad n = 0, 1, 2, \ldots \qquad \text{(A-6)}$$

which, to our knowledge, is not presented in the relevant

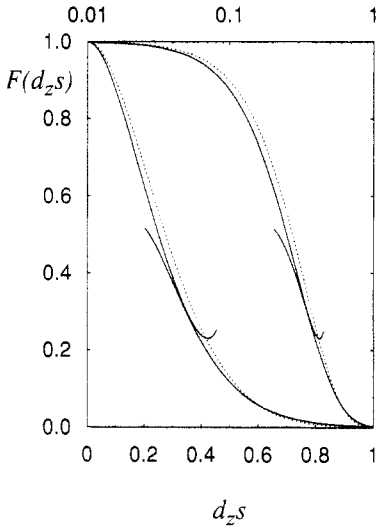

Figure 13. Comparison of $F_{th}(d_z s)$ for the hyperbolic tangent and $F_{erf}(d_z s)$ for the error function density profile. The lower set of curves are plotted on a linear scale and the upper set of curves on a semilogarithmic scale. Solid curves are plotted from eq A-7, truncated at $n = 4$, and from eq A-8. The empirical approximation (A-8) cannot be distinguished from the solid line within the resolution of the graphics.

tables or textbooks. It can be shown by comparing the residues of $\Gamma^2(z)\,\zeta(2z-2)$ and the expression resulting after applying the reflection formula for the ζ-function[31] $\zeta(z) = \zeta(1-z)\,\pi^{z-1/2}\Gamma[(1-z)/2]/\Gamma(z/2)$. The resulting power series expansion for $F(s)$ is given by

$$F(x=\pi^2 d_z s/2) = 1 - \frac{2}{3}x^2 + \frac{4}{\pi}\sum_{n=0}^{\infty}\frac{1+n}{1/2+n}\frac{(3/2)_n}{n!}\zeta(3+2n)(-1)^n\left(\frac{x}{\pi}\right)^{3+2n}, \quad |x| < \pi \quad \text{(A-7)}$$

where $(a)_n$ is Pochhammer's factorial. After truncating the sum, (A-7) can also serve as a computable representation for not too large argument.

Since the integrand in (A-4) has no right-hand poles, we expect $F(s)$ to have an exponentially small asymptotic expansion which can be computed using standard procedures.[32] The result up to first order in s^{-1} is given by

$$F(x=\pi^2 d_z s/2) \sim 8\pi^{-1/2}x^{3/2}\exp(-2x)\left[1 - \frac{5}{32x} + O(x^{-2})\right] \quad \text{(A-8)}$$

It is interesting to note that the leading term in (A-8) is, apart from the numerical values of the parameters, similar to the empirical approximation proposed by Roe[33] which, in terms of our definition, is given by $F(s) \simeq 4.2x^{1.2}\exp(-1.9x)$.

While (A-7) and (A-8) give us some insight into the analytical properties of $F(s)$, it will be useful for practical purposes to have a handy expression with a few parameters which approximates $F(s)$ reasonably well. Such an expression is given by

$$\tilde{F}(d_z s) \simeq [1 + (d_z s/a)^b]^{-c} \quad \text{(A-9)}$$

with $a = 0.801\,411$, $b = 1.833\,12$, and $c = 6.173\,42$. The absolute error of this approximation is $|\tilde{F} - F| < 0.0018$ over the whole range. The relative error will, of course, grow at large argument since (A-9) shows only algebraic decay.

Figure 13 shows a comparison of $F_{th}(d_z s)$ for the hyperbolic tangent and $F_{erf}(d_z s)$ for the error function density profile.

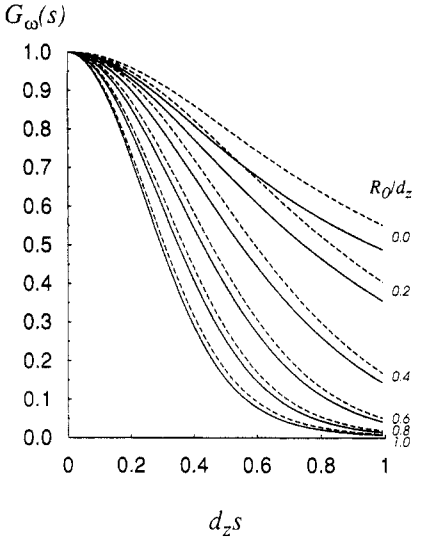

Figure 14. Comparison of G_ω^{th} for the hyperbolic tangent and G_ω^{erf} for the error function density profile. The solid curves are plotted from eq B-1 and the dashed curves from eq 13.

Appendix B

In analogy to an earlier work,[12] we obtain the following expression

$$I_z(s) = \frac{(\rho_1 - \rho_2)^2 S A_0 \pi^2 d_z^{\,2}}{16} G_\omega^{th}(s)$$

where

$$G_\omega^{th}(s) = 3e^{-a}\int_0^1 dz\, e^{-az^2}\left[\frac{1 - bz^2\,\mathrm{csch}^2(b^{1/2}z)}{bz^2}\right] \quad \text{(B-1)}$$

with $a = (\pi R_0 s)^2$ and $b = (\pi^2 d_z s/2)^2$. The integral can be solved, e.g., after series expansion. The leading terms of the resulting double sum are

$$G_\omega^{th}(s) = 1 - \frac{2a}{3} - \frac{b}{15} + O(a^2, b^2, ab)$$

The asymptotic expansion for large values of s is given by

$$G_\omega^{th}(s) \propto 3/2ab$$

Figure 14 shows a comparison of G_ω^{th} for the hyperbolic tangent and G_ω^{erf} for the error function density profile. The deviation between these two functions is relatively small in the range $R_0/d_z \simeq 0.9$ relevant for the present study.

References and Notes

(1) Wolff, T.; Burger, C.; Ruland, W. *Macromolecules* **1993**, *26*, 1707.
(2) Semenov, A. N. *Sov. Phys. JETP* **1985**, *61*, 733.
(3) Semenov, A. N. *Macromolecules* **1993**, *26*, 6617.
(4) Helfand, E.; Wasserman, Z. *Developments in Block Copolymers*; Goodman, I., Ed.; Applied Science: New York, 1982; Chapter 4.
(5) Helfand, E.; Wasserman, Z. *Macromolecules* **1976**, *9*, 879.
(6) Helfand, E.; Wasserman, Z. *Macromolecules* **1978**, *11*, 960.
(7) Helfand, E.; Wasserman, Z. *Macromolecules* **1980**, *13*, 994.
(8) Leibler, L. *Macromolecules* **1980**, *13*, 1602.
(9) Bates, F. S.; Rosedale, J. H.; Fredrickson, G. H. *J. Chem. Phys.* **1990**, *92*, 6255.
(10) Ruland, W. *Colloid Polym. Sci.* **1977**, *255*, 417.
(11) Siemann, U.; Ruland, W. *Colloid Polym. Sci.* **1982**, *260*, 999.

(12) Ruland, W. *Macromolecules* **1987**, *20*, 87.
(13) Hashimoto, T.; Shibayama, M.; Kawai, H. *Macromolecules* **1980**, *13*, 1237.
(14) Shibayama, M.; Hashimoto, T. *Macromolecules* **1986**, *19*, 740.
(15) Sakurai, S.; Okamoto, S.; Kawamura, T.; Hashimoto, T. *J. Appl. Crystallogr.* **1991**, *24*, 679.
(16) Porod, G. *Kolloid Z. Z. Polym.* **1951**, *124*, 83.
(17) Tsvankin, D. Ya.; Zubov, A. Yu.; Kitaigorodskii, A. I. *J. Polym. Sci.* **1968**, *C16*, 4081.
(18) In Hosemann, R.; Bagchi, S. N. *Direct Analysis of Diffraction by Matter*; North-Holland Publishing Co.: Amsterdam, The Netherlands, 1962, this equation is cited with the reference *Recl. Trav. Chim. Pays-Bas* **1944**, *63*, 5. This reference is incorrect. The only paper of J. J. Hermans to be found in *Recl. Trav. Chim. Pays-Bas* **1944**, *63*, has the reference *Recl. Trav. Chim. Pays-Bas* **1944**, *63*, 211. In this paper J. J. Hermans treats a problem similar but not equal to the lamellar system.
(19) Perret, R.; Ruland, W. *Kolloid Z. Z. Polym.* **1971**, *247*, 835.
(20) Ruland, W. *J. Appl. Crystallogr.* **1971**, *4*, 70.
(21) Shull, K. R. *Macromolecules* **1992**, *25*, 2122.
(22) Wiegand, W.; Ruland, W. *Colloid Polym. Sci.* **1979**, *66*, 355.
(23) Svergun, D. I.; Semenyuk, A. V.; Feigin, L. A. *Acta Crystallogr.* **1988**, *A44*, 244.
(24) Brandrup, J.; Immergut, E. H. *Polymer Handbook*; Wiley: New York, 1975.
(25) McMullen, W. E. *Macromolecules* **1993**, *26*, 1027.
(26) Melenkevitz, J.; Muthukumar, M. *Macromolecules* **1991**, *24*, 4199.
(27) Mayes, A. M.; Olvera de la Cruz, M. *Macromolecules* **1991**, *24*, 3975.
(28) Semenov, A. N. *Macromolecules*, in press.
(29) Abramowitz, M.; Stegun, I. A. *Handbook of Mathematical Functions*; Dover Publications: New York, 1965.
(30) Erdèlyi, A.; Magnus, W.; Oberhettinger, F.; Tricomi, F. G. *Tables of Integral Transforms*; McGraw-Hill: New York, 1954.
(31) Gradshteyn, I. S.; Ryzhik, I. M. *Tables of Integrals, Series and Products*; Academic Press: New York, 1965.
(32) Braaksma, B. L. J. *Comp. Math.* **1963**, *15*, 239.
(33) Roe, R.-J. *J. Appl. Crystallogr.* **1982**, *15*, 182.